A modular RNA interference system for gene regulation and robust dynamic feedback control

Ari Dwijayanti[1,3], Marko Storch[1,3,4], Guy-Bart Stan[2,3]*, Geoff S. Baldwin[1,3]*

[1] Department of Life Sciences, Imperial College London, London SW7 2AZ, United Kingdom

[2] Department of Bioengineering, Imperial College London, London SW7 2AZ, United Kingdom

[3] Imperial College Centre for Synthetic Biology, Imperial College London, London SW7 2AZ, United Kingdom

[4] London BioFoundry, Imperial College Translation & Innovation Hub, White City Campus, 80 Wood Lane, London W12 0BZ, United Kingdom

* To whom correspondence should be addressed. Email: g.baldwin@imperial.ac.uk; g.stan@imperial.ac.uk

Keywords: sRNA; post-transcriptional regulation; feedback control; modular design; synthetic biology

Abstract

The behaviour of engineered biological systems can be subject to deviation from design due to unpredictable changes in growth conditions, host response and metabolic load. Control engineering approaches are key to automatically maintain robust performance of designed systems despite such variations. RNA-controlled gene expression creates new possibilities for systematic, fast-responding and resource-efficient implementations of synthetic biology systems in living cells. Here, we demonstrate that a rational, modular design framework can provide an extensible platform for **m**odular **A**rtificial **R**NA **i**nterference (mARi) for robust, portable and multiplexed post-transcriptional regulation in *Escherichia coli.* We used mARi to construct a host-aware negative feedback control system that regulated protein production in response to cellular stress. We demonstrated that this mARi-based feedback control system resulted in an improvement in protein production up to 5-fold and was robust to perturbations in temperature, medium, scale, cell strain and gene product without further tuning. We anticipate that the use of robust RNA-based genetic control within an extensible DNA assembly framework, such as mARi, will have widespread applications in the realisation of sophisticated engineered biological systems, where dynamic regulation can provide improvements in gene circuit stability and microbial production.

Main

Cells use complex regulatory networks to appropriately sense, respond, and adapt to changes in their internal states and environment. One widely employed mechanism for adaptation relies on post-transcriptional regulation via small RNAs (sRNAs)[1,2]. sRNAs facilitate rapid, reversible, dynamic, and efficient signal propagation and typically act to coordinate and synchronize multiple signals through sequence-specific and transient RNA-RNA interactions[2,3], frequently leading to down-regulation of target gene expression[4]. In bacterial systems, *trans*-acting sRNAs rather than *cis*-acting sRNAs are reported to be especially effective in silencing gene expression due to their longer half-life[5].

The features of natural *trans*-encoded sRNAs have inspired versatile genetically encoded controllers for metabolic engineering and synthetic biology purposes[6–11]. sRNAs have a modular structure that lends itself to targeting of different genes. Specifically, the seed sequence that targets an mRNA can be altered to bind new targets, while retaining the native sRNA scaffold[12–14] (**Figs. 1a** and **2a**). The scaffold sequence is responsible for recognition by RNA chaperones, such as the host factor-1 (Hfq) protein. These abundant helper proteins are highly conserved in a range of organisms[15–18] as part of natural cellular regulation[19,20]. Use of endogenous regulatory machinery makes synthetic sRNA-based regulation portable, fast and lean when compared to other regulators such as transcription factors, zinc fingers, or CRISPRi, where the expression of accessory proteins creates delay, adds metabolic load and can cause toxicity[4,21–23].

Despite the fundamentally attractive features of sRNA-based regulatory systems, current approaches for implementing specific targeted artificial sRNAs are hampered by the need for bespoke design[7,9,12], leader sequences[13], or target insertions[6,8]. Here, we set out to design a universal, modular framework for the facile implementation of RNA-based control using verified, re-usable target sequences. To this effect, we used BASIC DNA assembly, which provides a modular, standardised framework for genetic structure based on orthogonal, computationally designed linkers[24].

Informed by the BASIC-derived gene architecture, we systematically designed, built, and characterised post-transcriptional regulation based on **m**odular **A**rtificial **R**NA **i**nterference (mARi) (**Fig. 1c**). The modular nature of the design enabled control of different genes and facilitates multiplexing of target genes. The system functioned across different *E. coli* strains and growth phases, demonstrating portability and robustness. By combining mARi with a stress-responsive promoter[25], we designed and built a dynamic, stress-driven, negative feedback system able to modulate the expression of stress-causing proteins at a post-transcriptional level. This host-aware feedback control increased overall yield and was robust to perturbations in host strains, conditions, and gene products.

Results

Design and implementation of a modular Artificial RNA interference regulation system

BASIC assembly relies on standardised linkers between interchangeable DNA parts (**Fig. 1a**,**b**)[24]. Expression cassettes and operons can be tuned using functional DNA linkers that encode a ribosome binding site (RBS) within a defined 5' untranslated region (UTR; UTR-RBS linker; **Fig. 1b**). Since BASIC UTRs are computationally designed to be orthogonal to the host genome and exclude secondary structure[26], they provide an ideal target for mARi (**Fig. 1c**).

mARi sequences were designed with two core components: the seed sequence that is complementary to the target sequence on an mRNA of interest and an sRNA scaffold for recruiting the RNA chaperone Hfq[27] (**Fig. 2a**). We chose the MicC scaffold, a native sRNA that regulates outer membrane protein (OmpC and OmpD) expression in *E. coli* via Hfq[28,29], as it was successfully used to construct artificial RNA interference systems[7,9,12,30]. To evaluate this approach, seed sequences were designed to target different positions in the translation initiation region of the mRNA (**Fig. 2b**). Positions 1-3 addressed gene-independent targets within the BASIC framework, while position 4 was specific to the GOI, *superfolder-gfp* (*sfgfp*; **Fig. 2b**). The reverse complements of the target sequences were combined with the MicC scaffold to create a series of mARi sequences (**Fig. 2a**).

To investigate the repression efficiency of mARi targets, sfGFP expression cassettes were assembled with P_{J23101_BASIC} and UTR-A-RBSc linker, while mARi expression was driven by P_{J23101} (**Fig. 1b**). Measurement of reporter expression demonstrated that all mARi target sequences led to repression of sfGFP, compared to the control lacking mARi (**Fig. 2c**). The intra-gene target at position 4 showed significant repression as anticipated[7,9,12]. However, targeting this position would require bespoke design and optimisation for each new expression cassette; a less desirable strategy from a modular engineering perspective. Position 1, which targets the UTR upstream of the RBS was as effective as position 4. Targeting this standardised UTR component of the BASIC framework is ideal for modular engineering since it is independent of both the GOI and RBS.

To evaluate the independence of position 1 UTR target, a set of constructs with 5 different RBS strengths (RBSa-RBSe) controlling sfGFP translation were assembled both with and without the position 1 mARi cassette. The *sfgfp* gene-only constructs resulted in a series of fluorescence intensities reflecting RBS strength variation (**Fig. 2d**). The position 1 UTR-targeted mARi cassette reduced the fluorescence signal in all cases (**Fig. 2d**). The relative repression remained constant across the series, demonstrating that the repression activity of mARi-A at position 1 was independent of RBS strength (**Fig. 2d**).

mARi activity is tuneable via genetic design parameters

With the underlying principle and design for modular RNA established, we sought to investigate the response of mARi to different genetic design parameters. We first investigated the relative abundance of mARi in relation to its target mRNA. The relative expression ratio for different promoter combinations was calculated by determining the relative strengths of the promoters used (**Supplementary Fig. 2b**). To assess the impact of the mARi:mRNA ratio, a matrix of designs with four different promoter strengths for both mARi and mRNA were constructed (**Fig. 3a,b**). The resulting sfGFP expression showed a consistent trend, with sfGFP fluorescence decreasing as the mARi:mRNA ratio increased (**Fig. 3c** and **Supplementary Fig. 2c**). The relative abundance of mARi in relation to its target mRNA is thus an important factor in repression, presumably because an excess of mARi is required to saturate binding of target mRNA.

A further variable affecting intracellular transcript abundance is copy number. Designs with different copy number plasmids were constructed using both high (blue box in **Fig. 3a**) and low (grey box in **Fig. 3a**) expression ratios to exemplify two different levels of transcript abundance. These systems were first assembled with both mARi and its target in a single plasmid, with varying plasmid copy numbers from low to high: pSC101, p15A and pMB1[31] (**Fig. 3d**). In all cases the high-expression ratio showed greater repression than the low-expression ratio (**Fig. 3e** and **Supplementary Fig. 4a**).

We next reasoned that by placing the mARi on a second, higher copy vector, repression should be more efficient. The mRNA expression cassette was placed on a p15A backbone, with mARi on higher copy pMB1 and pUC backbones (**Fig. 3d**), with both high- and low-expression ratios. Despite mARi being in excess, the double-plasmid systems all showed less repression than that observed with the corresponding single-plasmid systems (**Fig. 3f**). This suggests a role for spatial organization in post-transcriptional repression, as anticipated from recent theoretical analysis[32]. We hypothesize that tight spatial correlation of mARi and its target decreases their diffusion search space and hence their effective binding rate, thus competing with the alternative pathways of mRNA translation and mARi degradation.

mARi-based regulation is robust to different contexts

mARi-based gene regulation utilizes the native *E. coli* Hfq chaperone to regulate gene expression. The intracellular abundance of these components is influenced by several factors, including the genotype and growth phase of the host strain[33–35]. We therefore sought to evaluate the portability of this system between four commonly used *E. coli* strains: DH5α, DH10b, BL21(DE3), and BL21star(DE3). mARi constructs were transformed into each strain and the resulting sfGFP expression was evaluated as before. mARi was functional in all strains (**Fig. 3f**), and it was active across all phases of cell growth (**Fig. 3g**), although repression activity in the B strains was higher than in the K-12 strains **(Supplementary Fig. 4).** The mARi design lacks an RNase E cleavage site, and no difference on repression activity due to RNase E was observed in strains both with (BL21(DE3)) and without (BL21star(DE3)) RNase E **(Supplementary Fig. 4)**.

Modularity and orthogonality of mARi enables simultaneous, multiplexed gene regulation

The simultaneous regulation of multiple genes requires each gene to be addressed independently, and with minimal cross-talk between them. The standardised linker sequences that

define the UTR have been computationally generated to ensure their orthogonality in the DNA assembly process[26]. Computational evaluation of five selected UTR (UTR A-E) sequences demonstrated minimal similarity/identity scores between the set **(Supplementary Fig. 5a)** and the corresponding mARis (mARi A-E) were predicted to have minimal off-target interactions with three different *E. coli* genomes **(Supplementary Table 3).**

To evaluate target specificity, we constructed all possible combinations of mARi-A and target UTR upstream of *sfgfp*; in each case maintaining the same promoter and RBS (**Fig. 4a**). This demonstrated that significant repression was only observed between a given mARi and its cognate UTR (**Fig. 4b**).

Since the mARis exhibited specificity in the context of a single gene, we evaluated their ability to operate on two different genes simultaneously in a multiplexed design. Initially this was evaluated with both *sfgfp* and *mcherry* genes organised as separate transcriptional units (**Figs. 4c,d**). Specific and independent repression by each mARi towards its cognate target was observed, with UTR-A-*sfgfp* being selectively targeted by mARi-A and UTR-B-*mcherry* being targeted by mARi-B (**Fig. 4e** and **Supplementary Fig. 6a**).

A two-gene operon was then constructed with UTR-A-RBSc driving the expression of *sfgfp*, upstream of UTR-B-RBSc driving the expression of *mcherry* (**Fig. 4f**). With both genes on a single transcript, regulation of the upstream sfGFP follows a simple correlation to the cognate mARi-A; whilst the downstream mCherry is most strongly attenuated by its cognate mARi-B, it is also subject to transcriptional read-through, which is somewhat attenuated by mARi-A (**Fig. 4d** and **Supplementary Fig. 6b**).

Stress-driven mARi improves protein production yields by enabling host-responsive adaptation

Protein expression typically causes depletion of shared cellular resources, which can lead to reduced growth, diminished protein production yields or failure of designed circuits[36–40]. Negative

170 feedback systems are used in both engineering and biology to address this type of situation, where
171 robust performance is required despite perturbations and uncertainties[41,42]. The rapid and reversible
172 nature of RNA-based regulation makes it ideal as an actuator in biomolecular feedback control
173 systems[7,11,43]. We therefore sought to evaluate mARi as a dynamic negative feedback controller in
174 protein production, by placing the mARi system under control of the stress-inducible P_{htpG1} promoter[25].

175 A fusion protein of VioB and mCherry has previously been shown to trigger a host stress
176 response from P_{htpG1}, whilst enabling the simultaneous monitoring of expression levels by
177 fluorescence[25]. To validate P_{htpG1} activation, VioB-mCherry was placed under the control of an
178 inducible P_{Tet} promoter with both high and medium RBS strengths. A reporter plasmid with *sfgfp* under
179 the control of P_{htpG1} was used to determine the degree of P_{htpG1} response[25]. VioB-mCherry expression
180 leads to a response from P_{htpG1}-controlled sfGFP expression, which increases with increasing transcript
181 levels through induction of the Tet promoter with anhydrous tetracycline (aTc; **Supplementary Figs.**
182 **7,8**). The higher strength RBS caused a stronger P_{htpG1} response than the medium RBS at all induction
183 levels (**Supplementary Fig. 8**). Importantly, P_{htpG1} shows a progressive response to load
184 (**Supplementary Fig. 8**), a desirable characteristic for gain control in negative feedback.

185 Given the strong response of P_{htpG1} to VioB-mCherry, we sought to determine if a closed-loop
186 negative feedback system, whereby P_{htpG1} modulates VioB-mCherry production via an mARi actuator,
187 would increase the yield of protein production. A single plasmid system was assembled with the UTR-
188 A-VioB-mCherry being targeted by mARi-A, which was itself under the control of P_{htpG1} (**Fig. 5a**). The
189 equivalent plasmids lacking the mARi module were also constructed and both were transformed into
190 BL21(DE3).

191 mARi-based negative feedback improves the overall production of VioB-mCherry as seen by the
192 increase in total fluorescence, when compared to the system without mARi (**Fig. 5**). Feedback control
193 delivers increased protein expression per cell across all growth phases, but there is also an extension
194 of exponential growth, resulting in higher overall cell density (**Fig. 5c** and **Supplementary Fig. 9**):
195 single-cell analysis determined that increased fitness was not caused by non-producing mutants

(Supplementary Fig. 11). There was a notable shift in response to aTc induction of VioB-mCherry, with significantly improved expression per cell at lower levels of induction with mARi feedback (**Fig. 5b**), and overall up to a 5-fold increase in total protein (**Fig. 5c,d** and **Supplementary Fig. 9)**, confirmed by SDS-PAGE **(Supplementary Fig. 10).**

mARi-based negative feedback enables portable, robust and modular regulation across different contexts

A critical factor for the wide adoption of feedback control systems is the robust performance and portability they impart when used in different contexts and conditions. We therefore sought to test mARi-based negative feedback control under various perturbations, i.e. temperature, media, host strains, culture volume and GOI.

mARi-based negative feedback maintained the productivity improvement of VioB-mCherry at both 37°C and 30°C, over a 24 h incubation period (**Fig. 5e** and **Supplementary Fig. 13**). The improvement was also observed in different culture media and in different strains of *E. coli* (**Figs. 5c, d, f** and **Supplementary Figs. 12,14**). We also tested the performance of mARi-based negative feedback at different scales by comparing a 100 µl culture grown in 96 well-plate and a 50 ml culture grown in 250 ml shaking flasks. In both culture volumes the strains with mARi-based feedback exhibited a significant improvement of VioB-mCherry production, when compared to cells without mARi feedback (**Fig. 5g** and **Supplementary Fig. 15**).

To demonstrate the portability of the mARi-based feedback control systems, we deployed P_{htpG1}-mARi to control the expression of a different GOI (*lacz-mcherry*). The expression of LacZ-mCherry resulted in different P_{htpG1} activation, total protein production, and growth profiles, compared to the previous VioB-mCherry (**Supplementary Fig. 16**). Nonetheless, the mARi-based feedback system enhanced the productivity of LacZ-mCherry expression up to 2-fold compared to strains lacking the feedback (**Fig. 5h** and **Supplementary Fig. 17**). Remarkably, these productivity

221 improvements were achieved with no specific tuning of the system, beyond assembly of the GOI in
222 the BASIC framework with a UTR that is cognate to the mARi.
223

224 ## Discussion

225 Here we report the development, characterization, and implementation of a modular post-
226 transcriptional regulation system based on *trans*-acting small RNAs. Gene repression is achieved by
227 directing mARi to computationally designed, orthogonal UTR-RBS linkers in the BASIC DNA assembly
228 framework[24]. The target site was located upstream of the RBS and demonstrated effective repression
229 whilst being independent from both RBS and GOI contexts (**Fig. 2d** and **4**). The modular and orthogonal
230 nature of the design framework removes the need to design or insert bespoke target sites upstream
231 of target genes, a drawback of previous works focused on reusable *trans*-encoded small RNAs[6–8,11,13].
232 By directing mARi to the standardised UTR of the mRNA target, the RNA chaperone Hfq is
233 recruited to the translation initiation region of the mRNA. Hfq-mediated repression is thought to occur
234 either via steric occlusion of the RBS, preventing ribosome recruitment[28], or by facilitated active
235 degradation of the mRNA[29]. With the operon architecture that we investigated, there was clear
236 evidence that translation was attenuated by a combination of both target sites, with the effects being
237 largely independent and additive (**Fig. 4g**). This behaviour is consistent with steric hindrance of the
238 RBS being the main mode of action in the absence of an RNase E site. Facilitated degradation would
239 be expected to induce a similar repression level on both genes, whereas we observe that targeting of
240 the downstream gene has only a minor effect on the upstream gene (**Fig. 4g**). The enhanced repression
241 with occlusion of both UTR sites indicates that a bound sRNA is not completely effective as a roadblock
242 to ribosomes.
243 To evaluate the features of mARi, we characterised its responsiveness to design parameters and
244 robustness to different genetic contexts and conditions. Repression was modulated by both relative
245 transcript abundance and spatial organisation (**Fig. 3**). mARi proved to be a portable and robust
246 controller in different *E. coli* strains and across different growth phases (**Fig. 3**). We also demonstrated

247 that mARi can be multiplexed across multi-gene and operon systems (**Fig. 4**). This extensibility is
248 essential for the simultaneous regulation of multiple genes in metabolic engineering, layered genetic
249 control, and advanced genetic circuit applications.

250 We deployed mARi in a host-adaptive negative feedback system that responds to cellular stress
251 caused by protein over-expression. The heat-shock σ^{32}-dependent P_{htpG1} promoter was used as a stress
252 sensor[25]; while native Hfq is controlled by both σ^{32}-dependent and σ^{70}-dependent promoters, so it is
253 responsive to both growth and stress induced by protein misfolding[44]. Consequently, both the mARi
254 actuator and Hfq chaperone are activated by host stress in a bimolecular feedback control system.
255 Using P_{htpG1} as the sensor driving our mARi-actuated negative feedback reduced the translational load
256 in response to cellular stress. The resulting dynamic control optimised shared cellular resources,
257 leading to an increase in protein production up to 5-fold compared to without feedback (**Fig. 5d**).
258 Furthermore, the feedback control was robust to perturbations in temperature, media, culture
259 volume, as well as changes in host strains and gene products, without any further tuning of the system.

260 The ubiquity of sRNA control in biological systems demonstrates their importance in critically
261 important cellular processes of homeostasis and adaptation[1,11,45–47]. The programmability of sRNAs
262 makes them attractive candidates for the design of synthetic biological systems. Their fast and
263 dynamic response[4] makes them ideal sensors and actuators in both natural[45–48] and synthetic[7,11]
264 feedback control systems. Dynamic pathway regulation is an important application of biological
265 control engineering for the enhanced productivity and robustness of cellular production platforms[10,49–
266 53]. We have here demonstrated the applicability of mARi to improving protein production in a
267 feedback control system by adapting a native stress response to control the feedback circuit. The use
268 of alternative stress-responding promoters provides a mechanism for adapting this approach to
269 metabolic engineering applications[49], while the extensible modular framework and orthogonality of
270 mARi provide a platform for the rapid and efficient engineering of dynamic host-aware feedback
271 control biosystems for robust biomanufacturing and advanced genetic control applications.
272

Online Methods

Bacterial strains and growth conditions

The following *E. coli* strains were used for plasmid construction and expression: DH5α (F^- *endA1 glnV44 thi-1 recA1 relA1 gyrA96 deoR nupG purB20* ϕ80d*lacZ*ΔM15 Δ(*lacZYA-argF*)U169, hsdR17($r_K^- m_K^+$), λ^-), DH10b [F-*mcr*A Δ (*mrr-hsd*RMS-*mcr*BC) ϕ80*lac*ZΔM15 Δ*lac*X74 *rec*A1 *end*A1 *ara*D139 Δ (*ara leu*) 7697 *gal*U *gal*K *rps*L *nup*G λ-], BL21(DE3) (F^-*ompT hsd*S_B (r_B^-, m_B^-) *gal dcm* (DE3)), and BL21star(DE3) (F^-*ompT hsd*S_B (r_B^-, m_B^-) *gal dcm rne*131 (DE3)). *E. coli* colonies were grown from single-colony isolates in LB (Luria Bertani) medium supplemented with the appropriate antibiotic, shaken at 220 rpm and grown at 37°C (unless specified otherwise). The antibiotics used for plasmid maintenance were Chloramphenicol, Carbenicillin, and Kanamycin at a concentration of 25 µg/ml, 100 µg/ml and 50 µg/ml, respectively. Anhydrous tetracycline (aTc) from a stock concentration of 100 µg/ml in DMSO was used as an inducer.

Design and analysis of mARi sequences

The sequences of UTR-RBS linkers used in BASIC DNA assembly[24] were designed and validated using R2o DNA designer[26]. Secondary structures of the mARis were predicted using RNAFold WebServer (http://rna.tbi.univie.ac.at/cgi-bin/RNAWebSuite/RNAfold.cgi) and visualized using VARNA GUI[50] (http://varna.lri.fr/index.php?lang=en&page=tutorial&css=varna). The predicted interactions between mARis and their mRNA targets were simulated through IntaRNA[51,52] (http://rna.informatik.unifreiburg.de/IntaRNA/Input.jsp). The Free binding energy of mARi and its mRNA target site was estimated using a web-based service of the RNA folding software DINAMelt[53] (http://mfold.rna.albany.edu/?q=DINAMelt/Two-state-melting) using default parameters. The percent identity of mARi-UTR pairs was calculated using the EMBOSS needle method (https://www.ebi.ac.uk/Tools/psa/emboss_needle/). The predicted expression strength of the UTR-RBS linker was simulated using EMOPEC[54] and RBS calculator v2.0[55,56] with the input sequence starting from the Transcription Start Site (+1) to 100 bp of the downstream CDS. The off-target effect was

299 computed using CopraRNA[52,57,58] (http://rna.informatik.uni-freiburg.de/CopraRNA/Input.jsp).
300 NC_000913 (*E. coli* MG1655), NC_010473 (*E. coli* DH10b), NC_012892 and NC_012971 (*E. coli*
301 BL21(DE3)) were used as inputs references for host-background off-target prediction.
302
303 **Plasmid assembly**
304 Plasmids were constructed using the BASIC DNA assembly method[24,59]. New DNA parts with
305 prefix and suffix sequences were synthesised as gBlocks by Integrated DNA Technologies (IDT), or gene
306 fragments by TWIST Bioscience, or derived by PCR mutagenesis. The gBlocks and gene fragments were
307 directly cloned into pJET1.2 or pUC AmpR_plasmid as BASIC bioparts. Linkers for BASIC assembly were
308 provided by Biolegio or IDT **(Supplementary Table 5)**. All constructs were transformed into chemically
309 competent *E. coli* DH5α. Sequence verification of BASIC bioparts was carried out using Sanger
310 sequencing (Source Bioscience). PCR mutagenesis for generating new BASIC parts were carried out
311 using Phusion Polymerase (NEB) and phosphorylated oligonucleotides (IDT). Details of the BASIC
312 bioparts used to construct the plasmids are provided in **Supplementary Table 4**. Maps of plasmids
313 used in this study are provided in **Supplementary Fig. 18**.
314 The *viob-mcherry fusion* gene was extracted from plasmid pSB1C3-H3[25] (Addgene plasmid #
315 109381; http://n2t.net/addgene:109381; RRID:Addgene 109381) using a touchdown PCR method.
316 Briefly, target DNA was amplified using 10 µl of 5X HF Buffer, 1 µl of 10mM of dNTPs 10 mM, 2.5 µl of
317 forward primer 10 µM, 2.5 µl of reverse primer 10 µM, 50 pg of template DNA, 0.5 µl DNA Phusion
318 Polymerase (NEB), and ddH_2O up to 50 µl. A pair of primers, forward (5'-
319 tctggtgggtctctgtccatgagcattctggatttcccgcgtat-3') and reverse (5'-
320 cgataggtctcccgagccttaggtggagtggcggccctcg-3') were used to amplify specific region flanking *viob-*
321 *mcherry* gene with BASIC prefix and suffix. The following touchdown PCR protocol in the thermal cycler
322 was used for site-directed mutagenesis; (1) 95°C for 3 min, start loop 25 cycles, (2) 95°C for 30 sec, (3)
323 gradient from 65 to 70°C for 30 sec, (4) 72°C for 2 min, close loop, (5) 72°C for 10 min, and (6) 4°C hold
324 forever. The PCR product was then confirmed through gel agarose electrophoresis. Subsequently, a

325 gel purification was performed to a band with a size of ~3.7 kb. The purified DNA fragment was then
326 assembled by BASIC with methylated iP and iS linkers (Biolegio) into a pUC-AmpR backbone to create
327 a *viob-mcherry* fusion as a BASIC biopart.

328 The *lacz* gene was extracted from *E. coli* BL21(DE3) genome using touchdown PCR. The template
329 for fragment amplification was obtained from a single colony of BL21(DE3) diluted into 50 µl of dH_2O.
330 A pair of primers, forward (5'-tctggtgggtctctgtccatgaccatgattacggattcactggccgtc-3') and reverse (5'-
331 cgataggtctcccgagccttttttgacaccagaccaactggtaatggta-3') were used to amplify specific region flanking
332 the *lacz* gene with BASIC prefix and suffix. The PCR product was then confirmed through gel agarose
333 electrophoresis. Subsequently, a gel purification was performed to a band with a size of ~3 kb. The
334 purified DNA fragment was used to create a *lacz-mcherry* fusion in BASIC format by assembling the
335 *lacz* and *mcherry* with a fusion linker (FL2; **Supplementary Table 5**) into a pUC-AmpR backbone,
336 flanked by methylated iP and iS BASIC linkers (Biolegio).

337 A P_{htpG1}-sfGFP plasmid was used to detect the host-stress caused by overexpression of
338 recombinant protein (Addgene plasmid # 109387; http://n2t.net/addgene:109387;
339 RRID:Addgene_109387).

340

341 **Flow cytometry assay**

342 Cellular expression of sfGFP and mCherry was performed in 96 well plates with biological
343 triplicates for each construct. *E. coli* carrying an empty backbone (containing only an origin of
344 replication and an antibiotic resistance gene) was used as a negative control. *E. coli* colonies were
345 inoculated from glycerol stock into LB media supplemented with appropriate antibiotics. The colonies
346 were grown for 13 h at 30°C and 600 rpm in a benchtop shaker (Mikura). The culture was then diluted
347 200x (10 µl into 190 µl, then 10 µl into 90 µl) in LB media using an automated liquid handling robot
348 (CyBio Felix). The plate was grown at 37°C and 600 rpm in a benchtop shaker (Mikura). After 6 h of
349 incubation, the Abs600 was measured. Abs600 typically reached values in the range 0.6–0.7. Two
350 microliters of liquid culture were taken and diluted into 200 µl Phosphate Buffer Saline (PBS)

351 supplemented with 2 mg/ml Kanamycin. The fluorescence data of single cells was collected using a BD
352 Fortessa flow cytometer. The flow cytometer settings used were: 650 volts for forward scattered (FSC),
353 225 volts for side scattered (SSC), 520 volts for Alexa Fluor 488, 500 volts for mCherry and threshold
354 1200 for FSC and 200 SSC. In total 10,000 events were collected for each sample. The data was stored
355 as an FCS file 3.0 and analysis was done using FlowJo V10. Single cell population gating was performed
356 after plotting FSC-H against SSC-H and histograms of Alexa Fluor and mCherry channel of fluorescence.
357 The chosen gating covered 90-98% of the total population. The fluorescence intensity of the sample
358 was calculated by subtracting the geometric mean fluorescence of the control (strains with empty
359 backbone). The normalised fluorescence was calculated by dividing the fluorescence intensity of the
360 sample with mARi by the fluorescence of the sample without mARi expression.
361
362 **Plate reader assay**
363 For continuous growth assay, samples were first diluted 200x in LB media, then the plate was
364 incubated in a microplate reader (Clariostar, BMG Labtech) with continuous shaking at 37°C and 600
365 rpm for 12-24 h. Absorbance at 600 nm, GFP fluorescence (F:482-16/F:530-40) and RFP fluorescence
366 (F:540-20/F:590-20) were measured every 15 min. The normalised Abs600 was calculated by
367 subtracting the mean Abs600 of media only control from the Abs600 of each well. The fluorescence
368 intensity was corrected by subtracting the mean fluorescence value of negative control at equivalent
369 Abs600. The value Fl/Abs600 was calculated by dividing the value of corrected fluorescence by
370 corrected Abs600.
371
372 **P_{htpG1} response assay**
373 For the measurement of P_{htpG1} activity, BL21(DE3) cells carrying VioB-mCherry inducible
374 expression plasmid and P_{htpG1}-sfGFP plasmid, were cultured for 13 h at 30°C and 600 rpm in a benchtop
375 shaker (Mikura). After 200x dilution, plates were grown for outgrowth at 37°C with agitation at 600
376 rpm for 1 h and aTc inducer was added. The plate was placed in a microplate reader followed by

377 continuous incubation with continuous shaking at 37°C and 600 rpm for 12-24 h. Absorbance at 600
378 nm, sfGFP fluorescence (F:482-16/F:530-40) and mCherry fluorescence (F:540-20/F:590-20) were
379 measured continuously every 15 min. The normalised Abs600 was calculated by subtracting the mean
380 Abs600 of media only control from the Abs600 of each well. The fluorescence intensity was corrected
381 by subtracting the mean fluorescence value of negative control at equivalent Abs600. The value
382 Fl/Abs600 was calculated by dividing the value of corrected fluorescence by corrected Abs600.
383
384 **Measurement of VioB-mCherry and LacZ-mCherry production**
385 For the inducible expression of the recombinant protein assay, cells carrying inducible
386 expression plasmid with and without P_{htpG1}-mARi, were cultured for 13 h at 30°C and 600 rpm in a
387 benchtop shaker (Mikura). After 200x dilution, plates were grown for outgrowth at 37°C with agitation
388 at 600 rpm for 1 h and aTc inducer was added. Absorbance at 600 nm and mCherry fluorescence
389 (F:540-20/F:590-20) were measured continuously every 15 min. The normalised Abs600 was
390 calculated by subtracting the mean Abs600 of media only control from the Abs600 of each well. The
391 fluorescence intensity was corrected by subtracting the mean fluorescence value of negative control
392 at equivalent Abs600. The value Fl/Abs600 was calculated by dividing the value of corrected
393 fluorescence by corrected Abs600.
394 During continuous measurement of VioB-mCherry, 2 microliters of liquid culture were taken
395 at 6 h, 12 h, and 26 h post-induction. The samples were diluted into 200 µl Phosphate Buffer Saline
396 (PBS) supplemented with 2 mg/ml Kanamycin. The PBS-diluted samples were analysed on an Attune
397 NxT flow cytometer to obtain single-cell data. The flow cytometer settings used were as follows: 500
398 volts for forward scattered (FSC), 420 volts for side scattered (SSC), 550 volts for yellow light (YL), and
399 a threshold of 0.3x1000. In total 10,000 events were collected for each sample. The data was stored
400 as an FCS file 3.0 and analysis was done using FlowJo V10. Single cell population gating was performed
401 after plotting FSC-H against SSC-H and histograms of YL2 channel of fluorescence.

402 For assays in different host strains, the mARi-based negative feedback circuits (open and closed
403 loop) were propagated into BL21(DE3) and DH10b cells. Both engineered strains were incubated in LB
404 medium at 37°C and 600 rpm. aTc inducer with different concentration (0-100 ng/ml for BL21(DE3)
405 cells and 0-10 ng/ml for DH10b cells) was added after 1 h of outgrowth.
406 For different growth temperatures, the DH10b cell containing VioB-mCherry expression
407 plasmids with and without mARi were incubated at 30°C or 37°C in LB medium. To induce the
408 expression of VioB-mCherry, 5 ng/ml aTc inducer was added after 1 h of outgrowth. The plates were
409 incubated in a microplate reader with shaking at 600 rpm for 24 h post-induction.
410 For different growth media, the engineered DH10b cell were tested in three mediums: LB, 2YT
411 supplemented with 4% (w/v) glucose, and EZ MOPS RDM supplemented with 4% glucose. After 1 h
412 outgrowth, 5 ng/ml aTc inducer was added. The plate was incubated at 30°C and 600 rpm for 24 h
413 post-induction.
414
415 **SDS-PAGE assay**
416 Confirmation of total VioB-mCherry production was done using SDS-PAGE[60]. An overnight
417 culture was diluted 200x in 10 ml LB media supplemented with Chloramphenicol. After 1 h outgrowth,
418 aTc inducer at final concentration 5 ng/ml was added. The culture was then grown at 37°C and 600
419 rpm for 12 h. 1 ml of each culture was normalised to an Abs600 of 1.0 and centrifuged (13,000 g for 1
420 min). 100 µl of 1 x SDS-loading buffer supplemented with beta-mercaptoethanol was added to the
421 pellet followed by 2 min vortexing and 5 min boiling at 99°C. 5 µl of sample mix was then loaded into
422 SDS-PAGE with a concentration of 12% for the separating gel and 5% for the stacking gel. After running
423 the gel at 100 V for 2 h in 1x SDS running buffer, the gel was stained with Coomassie Brilliant Blue
424 solution (1.2 mM Coomassie Blue R-250 dye, 45% Methanol, 10 % glacial acetic acid) followed by de-
425 staining (20 % methanol, 10 % glacial acetic acid). The gel image was captured using a Fuji LAS-3000
426 imaging system. The molecular weight of VioB-mCherry was calculated using Protein Molecular

Weight Calculator (https://www.sciencegateway.org/tools/proteinmw.htm). A full amino acid sequence of VioB-mCherry with 1244 residue sequence resulted in protein weight of 138.64 kDa.

Shake-flask growth

The DH10b cell containing VioB-mCherry expression plasmids with and without mARi were inoculated into 5 ml of LB media supplemented with Chloramphenicol. Cultures were grown overnight at 30°C before being diluted 200x in 50 ml LB media supplemented with Chloramphenicol, in 250 ml shake flasks. After 1 h outgrowth, aTc inducer at final concentration 5 ng/ml was added. The cultures were then grown at 30°C in a shaking incubator (Innova: 220 rpm) for 24 h. At the end of the experiment, absorbance at 600 nm and RFP fluorescence (F:540-20/F:590-20) were measured. 1 ml of culture was spun down to obtain a pellet for visualisation.

Author Contributions

A.D.: Designed and performed all experiments and data analysis and contributed to the experimental strategy and the writing of the manuscript.

M.S.: Contributed to the experimental strategy and design, assisted with the experiments and data interpretation and contributed to the writing of the manuscript.

G.-B.S.: Contributed to the experimental strategy, assisted with experimental design and data interpretation and contributed to the writing of the manuscript.

G.S.B.: Contributed to the experimental strategy, assisted with the experimental design and data interpretation and wrote the manuscript.

Competing interests

The authors declare no competing interests.

Acknowledgements

A.D. received a PhD scholarship from Indonesia Endowment Fund for Education (LPDP). G.-B.S. gratefully acknowledges the support of the UK EPSRC through the EPSRC Fellowship for Growth EP/M002187/1 and of the Royal Academy of Engineering through the Chair in Emerging Technology programme. The authors would like to thank Prof Tom Ellis (Department of Bioengineering, Imperial College London) for providing DNA template for the amplification of VioB-mCherry.

References

1. Storz, G., Vogel, J. & Wassarman, K. M. Regulation by Small RNAs in Bacteria: Expanding Frontiers. *Molecular Cell* (2011). doi:10.1016/j.molcel.2011.08.022
2. Beisel, C. L. & Storz, G. Base pairing small RNAs and their roles in global regulatory networks. *FEMS Microbiol. Rev.* **34**, 866–882 (2010).
3. Nitzan, M., Rehani, R. & Margalit, H. Integration of Bacterial Small RNAs in Regulatory Networks. *Annu. Rev. Biophys.* **46**, 131–148 (2017).
4. Levine, E., Zhang, Z., Kuhlman, T. & Hwa, T. Quantitative Characteristics of Gene Regulation by Small RNA. *PLoS Biol.* **5**, (2007).
5. Man, S., Cheng, R., Miao, C., Gong, Q., Gu, Y., Lu, X., Han, F. & Yu, W. Artificial trans-encoded small non-coding RNAs specifically silence the selected gene expression in bacteria. *Nucleic Acids Res.* **39**, e50–e50 (2011).
6. Ghodasara, A. & Voigt, C. A. Balancing gene expression without library construction via a reusable sRNA pool. *Nucleic Acids Res.* **45**, 8116–8127 (2017).
7. Kelly, C. L., Harris, A. W. K. K., Steel, H., Hancock, E. J., Heap, J. T. & Papachristodoulou, A. Synthetic negative feedback circuits using engineered small RNAs. *Nucleic Acids Res.* **46**, 9875–9889 (2018).
8. Ceroni, F., Furini, S., Stefan, A., Hochkoeppler, A. & Giordano, E. A synthetic post-transcriptional controller to explore the modular design of gene circuits. *ACS Synth. Biol.* **1**, 163–71 (2012).

479 9. Na, D., Yoo, S. M., Chung, H., Park, H., Park, J. H. & Lee, S. Y. Metabolic engineering of
480 Escherichia coli using synthetic small regulatory RNAs. *Nat. Biotechnol.* **31**, 170–174 (2013).
481 10. Boo, A., Ellis, T. & Stan, G. B. Host-aware synthetic biology. *Curr. Opin. Syst. Biol.* **14**, 66–72
482 (2019).
483 11. Huang, H. H., Qian, Y. & Del Vecchio, D. A quasi-integral controller for adaptation of genetic
484 modules to variable ribosome demand. *Nat. Commun.* **9**, 1–12 (2018).
485 12. Yoo, S. M., Na, D. & Lee, S. Y. Design and use of synthetic regulatory small RNAs to control gene
486 expression in Escherichia coli. *Nat. Protoc.* **8**, 1694–707 (2013).
487 13. Lahiry, A., Stimple, S. D., Wood, D. W. & Lease, R. A. Retargeting a Dual-Acting sRNA for Multiple
488 mRNA Transcript Regulation. *ACS Synth. Biol.* **6**, 648–658 (2017).
489 14. Sharma, V., Yamamura, A. & Yokobayashi, Y. Engineering artificial small RNAs for Conditional
490 gene silencing in escherichia coli. *ACS Synth. Biol.* **1**, 6–13 (2012).
491 15. Franze De Fernandez, M. T., Eoyang, L. & August, J. T. Factor fraction required for the synthesis
492 of bacteriophage Qβ-RNA. *Nature* **219**, 588–290 (1968).
493 16. Sun, T., Li, S., Song, X., Pei, G., Diao, J., Cui, J., Shi, M., Chen, L. & Zhang, W. Re-direction of
494 carbon flux to key precursor malonyl-CoA via artificial small RNAs in photosynthetic
495 Synechocystis sp. PCC 6803. *Biotechnol. Biofuels* **11**, 1–16 (2018).
496 17. Huis in 't Veld, R. A. G., Kramer, G., van der Ende, A., Speijer, D. & Pannekoek, Y. The Hfq regulon
497 of Neisseria meningitidis. *FEBS Open Bio* **7**, 777–788 (2017).
498 18. Puerta-Fernández, E. & Vioque, A. Hfq is required for optimal nitrate assimilation in the
499 cyanobacterium Anabaena sp. strain PCC 7120. *J. Bacteriol.* **193**, 3546–3555 (2011).
500 19. Vytvytska, O., Moll, I., Kaberdin, V. R., Gabain, A. Von & Bla, U. Hfq (HF1) stimulates ompA
501 mRNA decay by interfering with ribosome binding. 1109–1118 (2000).
502 20. Moll, I. & Bla, U. D. O. Translational autocontrol of the Escherichia coli hfq RNA chaperone
503 gene. 976–984 (2005). doi:10.1261/rna.2360205.crystallography
504 21. Zhang, S. & Voigt, C. A. Engineered dCas9 with reduced toxicity in bacteria: implications for

505 genetic circuit design. *Nucleic Acids Res.* **46**, 11115–11125 (2018).

506 22. Liu, Q., Schumacher, J., Wan, X., Lou, C. & Wang, B. Orthogonality and Burdens of Heterologous
507 and Gate Gene Circuits in E. coli. *ACS Synth. Biol.* **7**, 553–564 (2018).

508 23. Cho, S., Choe, D., Lee, E., Kim, S. C., Palsson, B. & Cho, B. K. High-Level dCas9 Expression Induces
509 Abnormal Cell Morphology in Escherichia coli. *ACS Synth. Biol.* **7**, 1085–1094 (2018).

510 24. Storch, M., Casini, A., Mackrow, B., Trewhitt, H., Ellis, T. & Baldwin, G. S. BASIC: a new Biopart
511 Assembly Standard provides accurate, single-tier DNA assembly for synthetic biology. *ACS*
512 *Synth. Biol.* 4–10 (2015). doi:10.1021/sb500356d

513 25. Ceroni, F., Boo, A., Furini, S., Gorochowski, T. E., Borkowski, O., Ladak, Y. N., Awan, A. R., Gilbert,
514 C., Stan, G. B. & Ellis, T. Burden-driven feedback control of gene expression. *Nat. Methods* **15**,
515 387–393 (2018).

516 26. Casini, A., Christodoulou, G., Freemont, P. S., Baldwin, G. S., Ellis, T. & MacDonald, J. T. R2oDNA
517 Designer: Computational design of biologically-neutral synthetic DNA sequences. *ACS Synth.*
518 *Biol.* 140131140734008 (2014). doi:10.1021/sb4001323

519 27. Updegrove, T. B., Zhang, A. & Storz, G. Hfq: The flexible RNA matchmaker. *Curr. Opin. Microbiol.*
520 **30**, 133–138 (2016).

521 28. Chen, S., Zhang, A., Blyn, L. B. & Storz, G. MicC , a Second Small-RNA Regulator of Omp Protein
522 Expression in Escherichia coli MicC , a Second Small-RNA Regulator of Omp Protein Expression
523 in Escherichia coli. *J. Bacteriol.* **186**, 6689–6697 (2004).

524 29. Pfeiffer, V., Papenfort, K., Lucchini, S. & Hinton, J. C. D. Coding sequence targeting by MicC RNA
525 reveals bacterial mRNA silencing downstream of translational initiation. **16**, (2009).

526 30. Hussein, R. & Lim, H. N. Direct comparison of small RNA and transcription factor signaling.
527 *Nucleic Acids Res.* **40**, 7269–7279 (2012).

528 31. Jahn, M., Vorpahl, C., Hübschmann, T., Harms, H. & Müller, S. Copy number variability of
529 expression plasmids determined by cell sorting and Droplet Digital PCR. *Microb. Cell Fact.* 1–
530 12 (2016). doi:10.1186/s12934-016-0610-8

531 32. Teimouri, H., Korkmazhan, E., Stavans, J. & Levine, E. Sub-cellular mRNA localization modulates
532 the regulation of gene expression by small RNAs in bacteria. *Phys. Biol.* **14**, (2017).
533 33. Yoon, S. H., Han, M., Jeong, H., Lee, C. H., Xia, X., Lee, D., Shim, J. H., Lee, S. Y., Oh, T. K. & Kim,
534 J. F. Comparative multi-omics systems analysis of Escherichia coli strains B and K-12. *Genome*
535 *Biol.* **13**, R37 (2012).
536 34. Kajitani, M., Kato, A., Wada, A., Inokuchi, Y. & Ishihama, A. Regulation of the Escherichia coli
537 hfq gene encoding the host factor for phage Q(β). *J. Bacteriol.* **176**, 531–534 (1994).
538 35. Moon, K. & Gottesman, S. Competition among Hfq-binding small RNAs in Escherichia coli. *Mol.*
539 *Microbiol.* **82**, 1545–1562 (2011).
540 36. Gorochowski, T. E., Avcilar-Kucukgoze, I., Bovenberg, R. A. L., Roubos, J. A. & Ignatova, Z. A
541 Minimal Model of Ribosome Allocation Dynamics Captures Trade-offs in Expression between
542 Endogenous and Synthetic Genes. *ACS Synth. Biol.* **5**, 710–720 (2016).
543 37. Scott, M., Klumpp, S., Mateescu, E. M. & Hwa, T. Emergence of robust growth laws from
544 optimal regulation of ribosome synthesis. *Mol. Syst. Biol.* **10**, 747–747 (2014).
545 38. Darlington, A. P. S., Kim, J., Jiménez, J. I. & Bates, D. G. Design of a translation resource
546 allocation controller to manage cellular resource limitations. *IFAC-PapersOnLine* **50**, 12653–
547 12660 (2017).
548 39. Carbonell-Ballestero, M., Garcia-Ramallo, E., Montañez, R., Rodriguez-Caso, C. & Macía, J.
549 Dealing with the genetic load in bacterial synthetic biology circuits: Convergences with the
550 Ohm's law. *Nucleic Acids Res.* **44**, 496–507 (2016).
551 40. Kafri, M., Metzl-Raz, E., Jona, G. & Barkai, N. The Cost of Protein Production. *Cell Rep.* **14**, 22–
552 31 (2016).
553 41. Reeves, G. T. & Fraser, S. E. Biological Systems from an Engineer's Point of View. *PLoS Biol.* **7**,
554 e1000021 (2009).
555 42. Becskei, A. & Serrano, L. Becskei Serrano Nature 2000 Autoregulation. *Nature* **405**, 590–593
556 (2000).

557 43. Stevens, J. T. & Carothers, J. M. Designing RNA-Based Genetic Control Systems for Efficient
558 Production from Engineered Metabolic Pathways. *ACS Synth. Biol.* **4**, 107–115 (2015).
559 44. Valentin-Hansen, P. & Eriksen, M. MicroReview The bacterial Sm-like protein Hfq : a key player
560 in RNA transactions. **51**, 1525–1533 (2004).
561 45. Thompson, K. M., Rhodius, V. A. & Gottesman, S. σE regulates and is regulated by a small RNA
562 in Escherichia coli. *J. Bacteriol.* **189**, 4243–4256 (2007).
563 46. Tu, K. C., Long, T., Svenningsen, S. L., Wingreen, N. S. & Bassler, B. L. Negative Feedback Loops
564 Involving Small Regulatory RNAs Precisely Control the Vibrio harveyi Quorum-Sensing
565 Response. *Mol. Cell* **37**, 567–579 (2010).
566 47. Brosse, A., Korobeinikova, A., Gottesman, S. & Guillier, M. Unexpected properties of sRNA
567 promoters allow feedback control via regulation of a two-component system. *Nucleic Acids*
568 *Res.* **44**, 9650–9666 (2016).
569 48. Kalamorz, F., Reichenbach, B., März, W., Rak, B. & Görke, B. Feedback control of glucosamine-
570 6-phosphate synthase GlmS expression depends on the small RNA GlmZ and involves the novel
571 protein YhbJ in Escherichia coli. *Mol. Microbiol.* **65**, 1518–1533 (2007).
572 49. Dahl, R. H., Zhang, F., Alonso-Gutierrez, J., Baidoo, E., Batth, T. S., Redding-Johanson, A. M.,
573 Petzold, C. J., Mukhopadhyay, A., Lee, T. S., Adams, P. D. & Keasling, J. D. Engineering dynamic
574 pathway regulation using stress-response promoters. *Nat. Biotechnol.* **31**, 1039–1046 (2013).
575 50. Darty, K., Denise, A. & Ponty, Y. VARNA : Interactive drawing and editing of the RNA secondary
576 structure. **25**, 1974–1975 (2009).
577 51. Busch, A., Richter, A. S. & Backofen, R. IntaRNA: Efficient prediction of bacterial sRNA targets
578 incorporating target site accessibility and seed regions. *Bioinformatics* **24**, 2849–2856 (2008).
579 52. Wright, P. R., Georg, J., Mann, M., Sorescu, D. A., Richter, A. S., Lott, S., Kleinkauf, R., Hess, W.
580 R. & Backofen, R. CopraRNA and IntaRNA: Predicting small RNA targets, networks and
581 interaction domains. *Nucleic Acids Res.* **42**, 119–123 (2014).
582 53. Markham, N. R. & Zuker, M. DINAMelt web server for nucleic acid melting prediction. *Nucleic*

583 *Acids Res.* **33**, 577–581 (2005).

584 54. Bonde, M. T., Pedersen, M., Klausen, M. S., Jensen, S. I., Wulff, T., Harrison, S., Nielsen, A. T.,
585 Herrgård, M. J. & Sommer, M. O. A. Predictable tuning of protein expression in bacteria. *Nat.*
586 *Methods* **13**, 233–236 (2016).

587 55. Salis, H. M., Mirsky, E. A. & Voigt, C. A. Automated design of synthetic ribosome binding sites
588 to control protein expression. *Nat. Biotechnol.* **27**, 946–950 (2009).

589 56. Espah Borujeni, A., Channarasappa, A. S. & Salis, H. M. Translation rate is controlled by coupled
590 trade-offs between site accessibility, selective RNA unfolding and sliding at upstream standby
591 sites. *Nucleic Acids Res.* **42**, 2646–2659 (2014).

592 57. Raden, M., Ali, S. M., Alkhnbashi, O. S., Busch, A., Costa, F., Davis, J. A., Eggenhofer, F.,
593 Gelhausen, R., Georg, J., Heyne, S., Hiller, M., Kundu, K., Kleinkauf, R., Lott, S. C., Mohamed, M.
594 M., Mattheis, A., Miladi, M., Richter, A. S., Will, S., Wolff, J., Wright, P. R. & Backofen, R. Freiburg
595 RNA tools: A central online resource for RNA-focused research and teaching. *Nucleic Acids Res.*
596 **46**, W25–W29 (2018).

597 58. Wright, P. R., Richter, A. S., Papenfort, K., Mann, M., Vogel, J., Hess, W. R., Backofen, R. & Georg,
598 J. Comparative genomics boosts target prediction for bacterial small RNAs. *Proc. Natl. Acad.*
599 *Sci.* **110**, E3487–E3496 (2013).

600 59. Storch, M., Casini, A., Mackrow, B., Ellis, T. & Baldwin, G. S. *BASIC: A simple and accurate*
601 *modular DNA assembly method*. *Methods in Molecular Biology* **1472**, (2017).

602 60. Sambrook, J. *Molecular cloning : a laboratory manual*. (Third edition. Cold Spring Harbor, N.Y. :
603 Cold Spring Harbor Laboratory Press, [2001] ©2001).

604

605

606

607

608

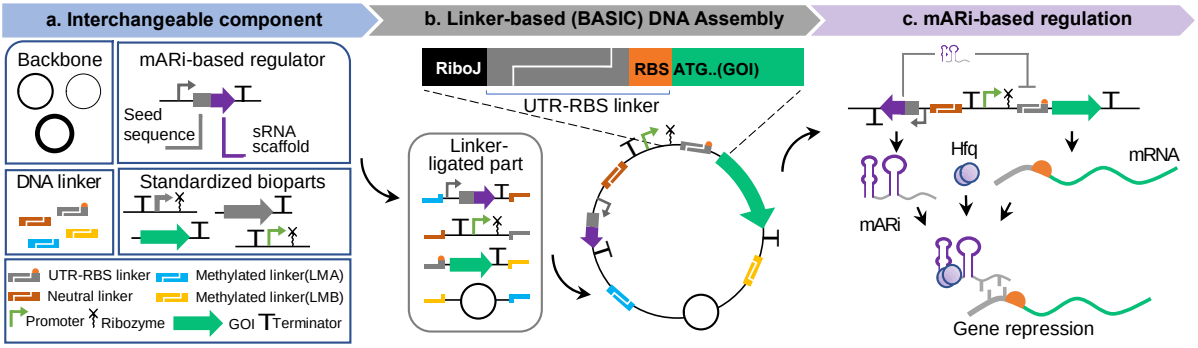

Fig. 1. mARi-based regulation integrated into the BASIC modular design-assembly framework. (**a**) BASIC DNA assembly is based on standardised DNA parts and computationally designed linkers: standardised backbones including Origin of Replication (ORI), antibiotic resistance, and bioparts; linkers are either neutral, encode UTR-RBS or are methylated to regenerate the BASIC prefix (LMA) and suffix (LMB) during assembly. mARi-based regulators were composed as BASIC parts consisting of a promoter, seed sequence (grey), sRNA scaffold (purple) and terminator. (**b**) Plasmids were constructed from the interchangeable DNA parts using BASIC DNA assembly[24]: a representative assembled plasmid shows a functional UTR-RBS linker controlling expression of a downstream gene of interest (GOI). (**c**) Expression of mARi leads to repression of a target gene with a cognate UTR by base-pairing between the 5'untranslated region and mARi seed sequence.

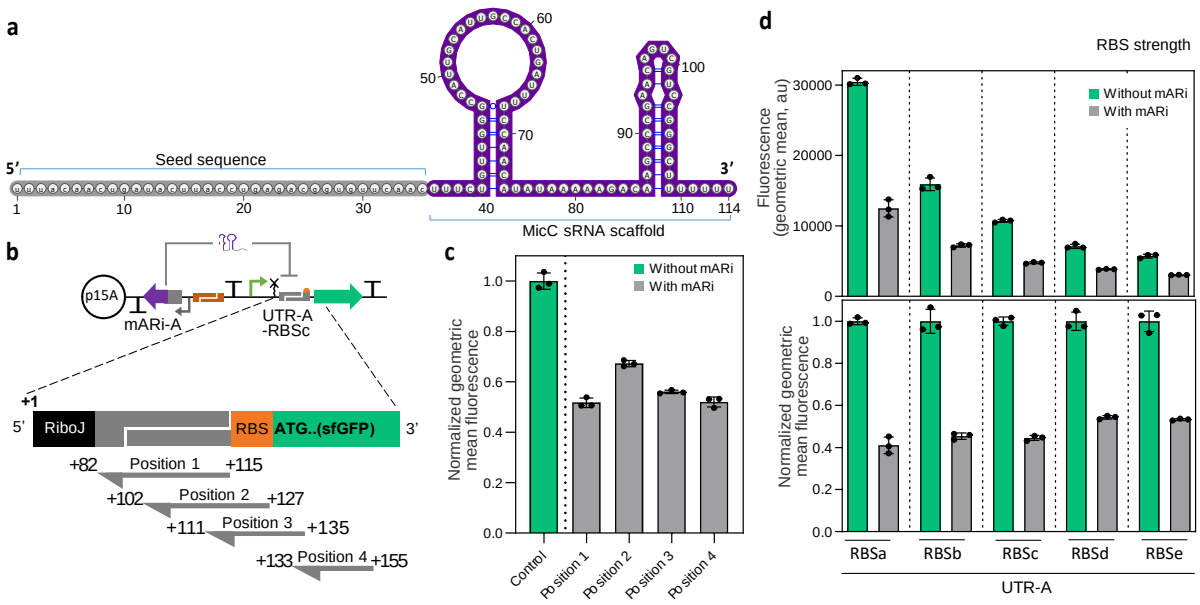

Fig. 2. Design and development of mARi-based gene regulation.

(**a**) Sequence and secondary structure of mARi containing a seed sequence (grey) and MicC RNA scaffold (purple). (**b**) Schematic design of target site selection of mARi-mediated repression. Four positions within the translation initiation region were selected as target sites (Positions 1-4; **Supplementary Table 1**). The numbers indicate the relative position of the mARi downstream of the transcription start site (+1). (**c**) Functional characterization of mARi-based gene regulation showing the silencing activity of mARi-A for the different target positions vs a sfGFP-only control without mARi. (**d**) The fluorescence intensity (top) and normalised fluorescence (bottom) when position 1 mARi-A was used to target UTR-A with varying RBS strength. All sfGFP fluorescence measurements were performed by flow cytometry after 6 h growth. Data are shown with error bars for the mean ± SD of triplicate measurements (black dots).

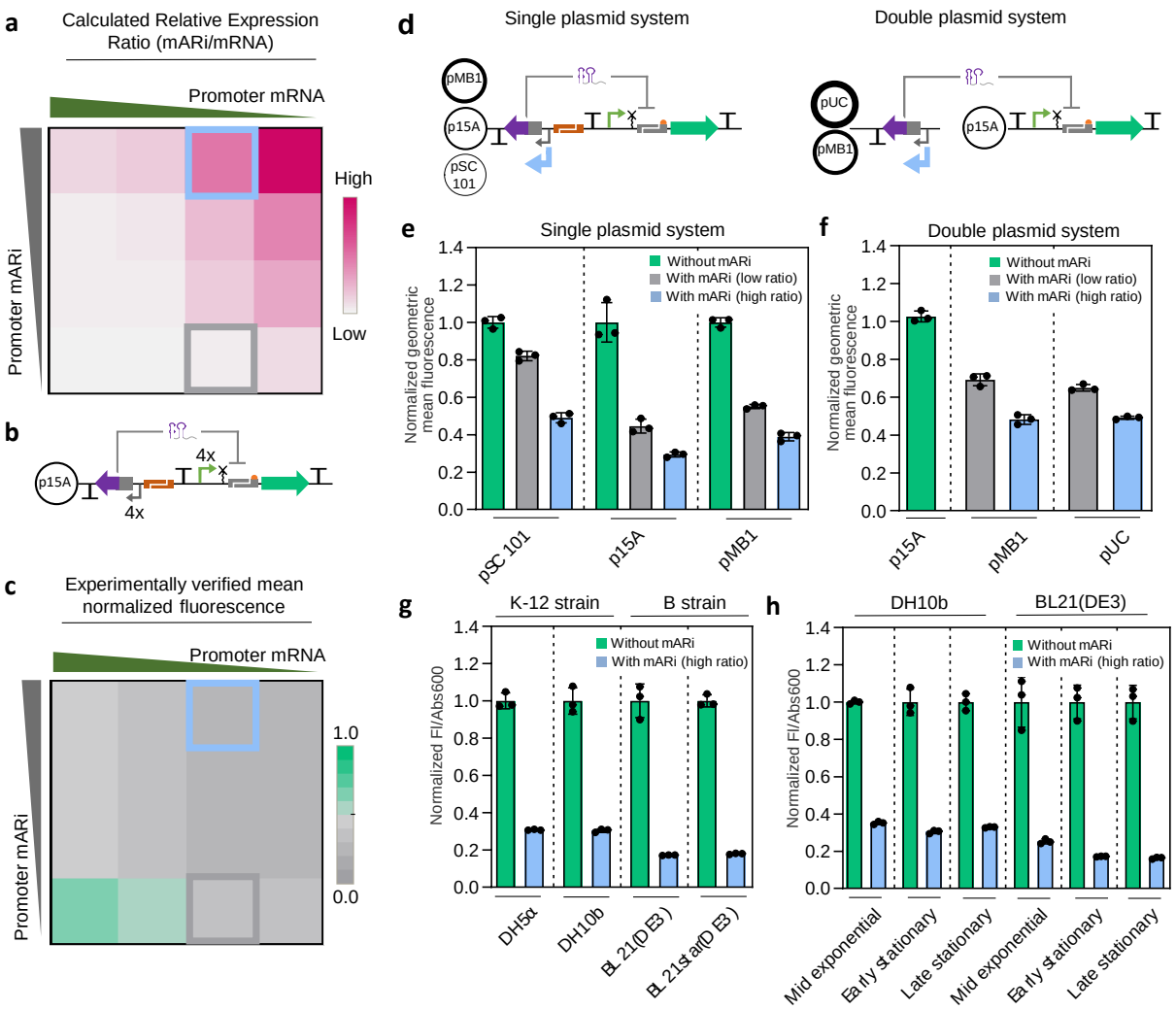

Fig. 3. Characterization of mARi-A across different genetic architectures.

(**a**) Heat-map showing relative expression ratio calculated from the relative strength of promoters driving mARi and mRNA expression across a matrix of constructs (**Supplementary Fig. 2b**). The representative conditions used for set-point high and low expression ratios are highlighted with a blue square (P_{J23119}-mARi:$P_{J23101BASIC}$-mRNA) and grey square (P_{J23101}-mARi:$P_{J23101BASIC}$-mRNA), respectively. (**b**) Schematic of mARi repression constructs used to investigate the effect of transcript ratio using four different strength constitutive promoters driving both mARi and mRNA in a single plasmid system. (**c**) Heat-map showing the measured relative expression levels (mean normalised fluorescence) of the mARi expression ratio matrix from (**a**). (**d**) Schematic of the mARi-based repression system with high and low expression ratios constructed in single- and double-plasmid systems with different copy numbers. Reporter expression was measured for the single (**e**) and double (**f**) plasmid systems for high

656 and low ratio mARi against a control construct without mARi; sfGFP fluorescence measurements were
657 performed by flow cytometry assay. (**g**) Reporter expression of the high-ratio mARi was measured in
658 different *E. coli* strains against a control construct without mARi. (**h**) The repression activity of mARi in
659 two representative strains (DH10b and BL21(DE3)) across three different growth phases
660 (**Supplementary Fig. 3**). Assays in **g** and **h** were performed by plate reader assay. All error bars show
661 the mean ± SD of triplicate measurements (black dots).
662
663
664
665
666
667
668
669
670

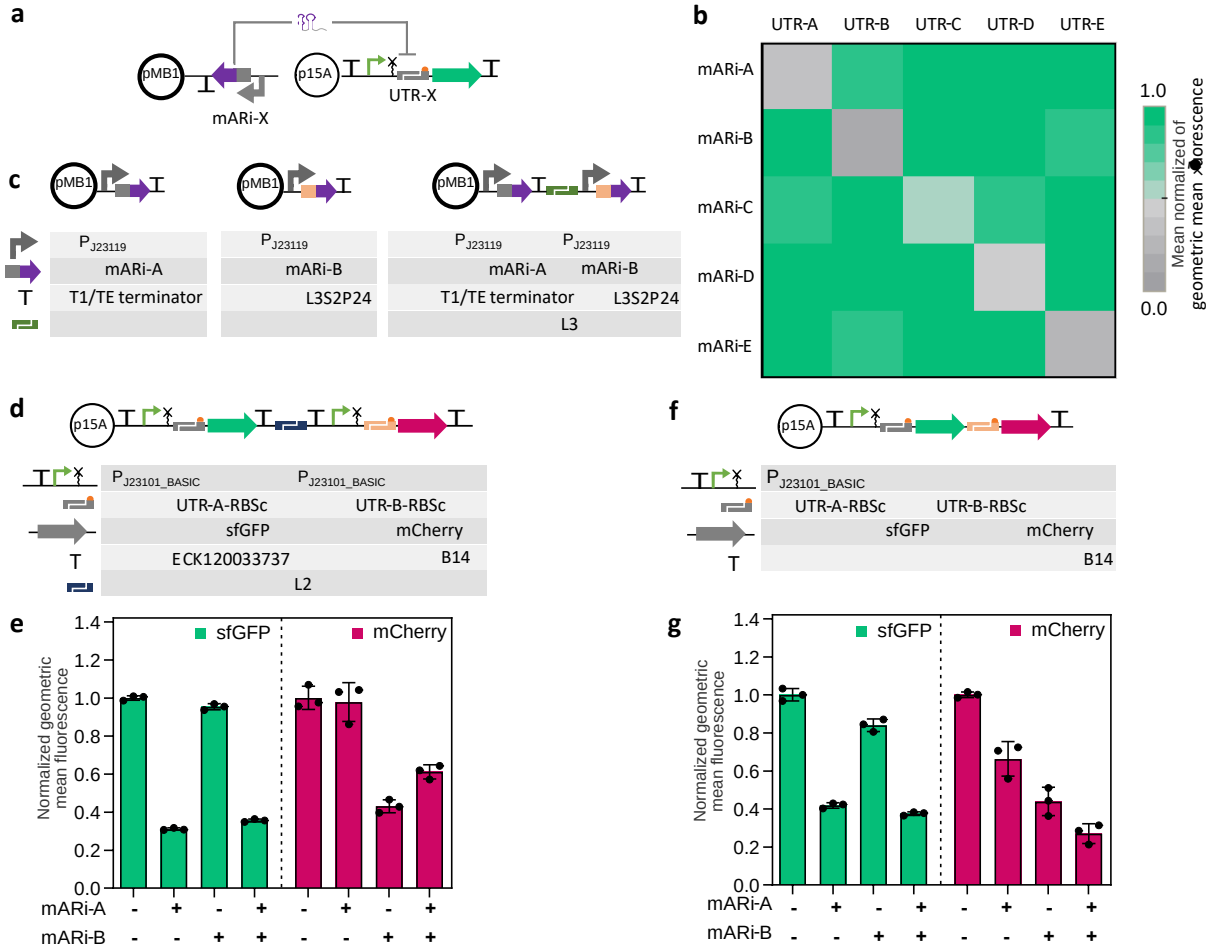

Fig. 4. mARi enables multiplex and simultaneous control of gene expression in a multi-gene system. (**a**) Schematic of experimental design to evaluate the target specificity of modular mARi-mRNA pairs. (**b**) Fluorescence response of matrix of all possible mARi/UTR pairs measured by flow cytometry assay with triplicate repeats (**Supplementary Fig. 5c**). (**c**) Schematic of mARi expression cassettes (mARi-A and/or mARi-B). (**d**) Schematic of reporters in dual transcription units. (**e**) The fluorescence response of dual reporters in a double transcriptional unit system when combined with all possible mARi-A and mARi-B regulators was measured by flow cytometry assay. **(f)** Schematic of dual reporters in an operon system. (**g**) The fluorescence response of dual reporters in an operon system when combined with all possible mARi-A and mARi-B regulators was measured by flow cytometry assay. All error bars show the mean ± SD of triplicate measurements (black dots).

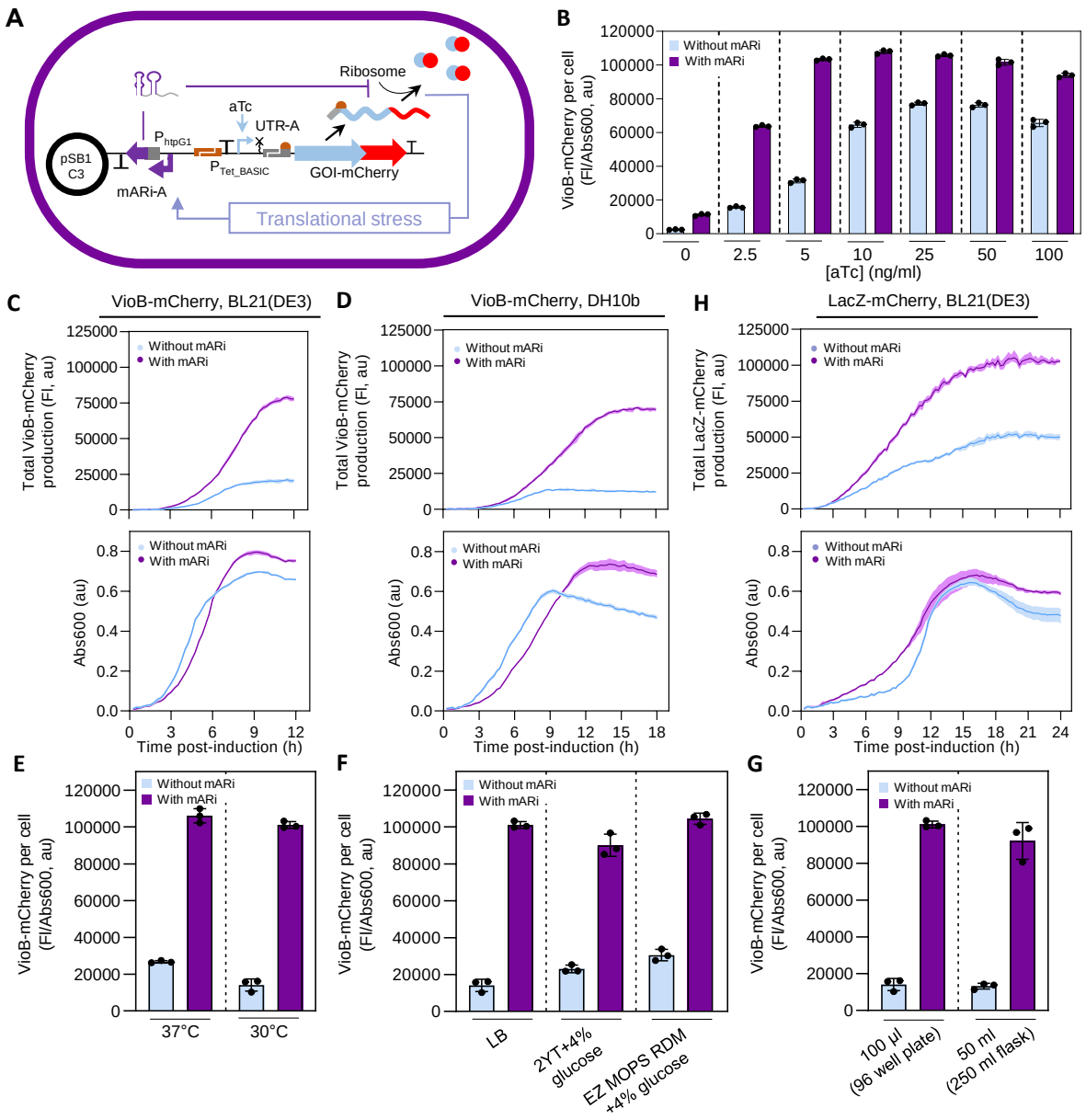

Fig. 5. Host-responsive mARi negative feedback robustly improves protein production.

(**a**) Schematic of the dynamic feedback control system in a single plasmid system; mARi-A is controlled by the host stress responsive P_{htpG1} promoter; GOI fused to mCherry under Tet-inducible promoter with UTR-A-RBSa in high copy number plasmid (pSB1C3). (**b**) VioB-mCherry production per cell as a function of aTc induction at 12 h post induction in BL21(DE3) was measured by plate-reader assay. (**c** and **d**) The accumulation of VioB-mCherry (top) and growth profile (bottom) over induction time with 5 ng/ml aTc in BL21(DE3) (**c**) and DH10b (**d**). (**e-g**) Expression of VioB-mCherry in BL21(DE3) was measured with 5 ng/ml aTc under different conditions of temperature (**e**); growth media (**f**) and culture volumes (**g**), measured by plate-reader assay after 24 h and in shake flask for (**g**). (**h**) The

694 accumulation of LacZ-mCherry (top) and growth profile (bottom) over induction time with 5 ng/ml aTc

695 in BL21(DE3). All error bars show the mean ± SD of triplicate measurements (black dots).